BIOLOGICAL CRYSTALLOGRAPHY
ISSN 1399-0047

Crystallographic studies of two variants of *Pseudomonas aeruginosa* IMPDH with impaired allosteric regulation

Gilles Labesse,[a,b]* Thomas Alexandre,[c,d,e]‡ Muriel Gelin,[a,b] Ahmed Haouz[f,g] and Hélène Munier-Lehmann[c,d]*

[a]CNRS, UMR5048, Université Montpellier 1 et 2, Centre de Biochimie Structurale, 34090 Montpellier, France, [b]INSERM U1054, Centre de Biochimie Structurale, 34090 Montpellier, France, [c]Unité de Chimie et Biocatalyse, Institut Pasteur, 75015 Paris, France, [d]CNRS, UMR3523, 75015 Paris, France, [e]Université Paris Descartes Sorbonne Paris Cité, Institut Pasteur, 75015 Paris, France, [f]Plateforme de Cristallographie, Département de Biologie Structurale et Chimie, Institut Pasteur, 75015 Paris, France, and [g]CNRS, UMR3528, 75015 Paris, France. *Correspondence e-mail: labesse@cbs.cnrs.fr, hmunier@pasteur.fr

Received 20 April 2015
Accepted 7 July 2015

Edited by R. McKenna, University of Florida, USA

‡ Present address: Department of Microbiology and Immunobiology, Harvard Medical School, Boston, MA 02115, USA.

Keywords: nucleotide metabolism; allosteric regulation; quaternary structure; CBS module; IMPDH.

PDB references: *Pseudomonas aeruginosa* IMPDH, ΔCBS variant, apo form, 5ahl; IMP-bound form, 5ahm; D199N variant, apo form, 5ahn

Supporting information: this article has supporting information at journals.iucr.org/d

Inosine-5′-monophosphate dehydrogenases (IMPDHs), which are the rate-limiting enzymes in guanosine-nucleotide biosynthesis, are important therapeutic targets. Despite in-depth functional and structural characterizations of various IMPDHs, the role of the Bateman domain containing two CBS motifs remains controversial. Their involvement in the allosteric regulation of *Pseudomonas aeruginosa* IMPDH by Mg-ATP has recently been reported. To better understand the function of IMPDH and the importance of the CBS motifs, the structure of a variant devoid of these modules (ΔCBS) was solved at high resolution in the apo form and in complex with IMP. In addition, a single amino-acid substitution variant, D199N, was also structurally characterized: the mutation corresponds to the autosomal dominant mutant D226N of human IMPDH1, which is responsible for the onset of the retinopathy adRP10. These new structures shed light onto the possible mechanism of regulation of the IMPDH enzymatic activity. In particular, three conserved loops seem to be key players in this regulation as they connect the tetramer–tetramer interface with the active site and show significant modification upon substrate binding.

1. Introduction

The key metabolic enzyme inosine-5′-monophosphate dehydrogenase (IMPDH) converts inosine 5′-monophosphate (IMP) to xanthosine 5′-monophosphate (XMP). This enzyme occupies a central role in the *de novo* synthesis of guanosine nucleotides (Hedstrom, 2009; Pankiewicz & Goldstein, 2003): its inhibition causes a reduction of the guanine-nucleotide pools and an imbalance between adenine and guanine nucleotides. Accordingly, IMPDHs have been the subject of various functional and structural studies and IMPDH inhibitors are used in the clinic in antiviral therapies (Nair & Shu, 2007) and immunosuppressive therapies (Chen & Pankiewicz, 2007; Ratcliffe, 2006). More recently, some antibacterial applications have been proposed (Hedstrom *et al.*, 2011).

To date, virtually all known IMPDHs have been reported as sharing a two-domain organization (Hedstrom, 2009; Pankiewicz & Goldstein, 2003) composed of a catalytic domain and a smaller flanking domain containing two CBS motifs (Bateman, 1997; Ereño-Orbea *et al.*, 2013). The exceptions are the IMPDHs from *Borrelia burgdorferi* and *Cryptosporidium*

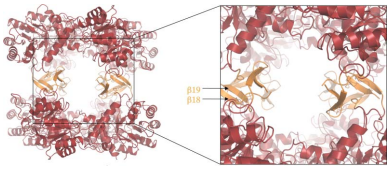

parvum, which do not contain CBS motifs. The catalytic domain has been well characterized by means of X-ray crystallography and biochemistry, and potent inhibitors targeting IMPDHs bind to this domain (Goldstein *et al.*, 2003; Shu & Nair, 2008). In contrast, the role of the CBS motifs is still unclear, since the deletion of these modules in human or *Escherichia coli* IMPDH has no effect on the catalytic activity (Nimmesgern *et al.*, 1999; Pimkin & Markham, 2008). On the other hand, in an *E. coli* strain harbouring a $guaB^{\Delta CBS}$ gene the regulation of the purine-nucleotide pools was dramatically affected (Pimkin & Markham, 2008). This strain is also sensitized to adenosine and inosine, leading to growth arrest on minimal media (Pimkin *et al.*, 2009). In the case of human IMPDH1, point mutations within the CBS motifs are associated with retinal degeneration and the severe retinopathy adRP10 (Aherne *et al.*, 2004; Bowne *et al.*, 2006; Kennan *et al.*, 2002). These mutations do not impact the catalytic activity, but decrease the affinity for single-stranded nucleic acids (Kozhevnikova *et al.*, 2012; Mortimer & Hedstrom, 2005) and can promote protein aggregation (Aherne *et al.*, 2004). Moreover, contradictory results have been reported regarding the role of the CBS motifs in ATP binding (Mortimer & Hedstrom, 2005; Pimkin & Markham, 2008; Pimkin *et al.*, 2009; Scott *et al.*, 2004; Thomas *et al.*, 2012). Although the physiological importance of the CBS motifs is obvious *in vivo*, the underlying molecular mechanisms involved in these processes remain to be elucidated.

We have recently demonstrated the binding of Mg-ATP to *Pseudomonas aeruginosa* IMPDH (IMPDHpa) and its crucial role in the regulation of the catalytic activity of the enzyme and its quaternary structure (Labesse *et al.*, 2013). We have depicted the ATP-binding sites within the two CBS motifs by means of X-ray crystallography and site-directed mutagenesis. In parallel, we have characterized the octameric organization of IMPDHpa in its ATP-bound and apo forms utilizing various biophysical techniques (SAXS, cryoelectron microscopy and analytical ultracentrifugation). In fact, similar octameric forms can be deduced from the crystal packing in most crystal structures of IMPDHs solved to date. Surprisingly, this structural feature was not taken into account in the analysis of the structure–function relationship.

Intriguingly, in the majority of the three-dimensional structures deposited in the PDB (Rose *et al.*, 2011) the CBS motifs were not visible in the electron-density maps, while the three-dimensional structures of deletion derivatives had not been described until recently (Makowska-Grzyska *et al.*, 2015). This prompted us to engage in a follow-up analysis of variants of IMPDHpa impaired in allosteric regulation.

Here, we describe the high-resolution structures of an IMPDHpa variant lacking the CBS motifs (ΔCBS) in the presence or absence of IMP. In addition, we have also solved the structure in the presence of IMP of the D199N variant, which mimics the mutant in the human IMPDH1 counterpart (D226N) that is responsible for the onset of adRP10 (Bowne *et al.*, 2002). We also discuss the distinct conformations of loops surrounding the active site and their role in substrate binding as well as their involvement in the octameric organization. This study suggests a mechanism for the allosteric regulation of IMPDH through the CBS motifs.

2. Materials and methods

2.1. Expression and purification of IMPDHpa

The expression and purification of IMPDHpa variants have recently been described (Labesse *et al.*, 2013). Briefly, the recombinant proteins expressed in *E. coli* were purified using a two-step procedure involving affinity chromatography followed by size-exclusion chromatography. They were stored in buffer *A* (20 m*M* potassium phosphate pH 8, 25 m*M* KCl). Enzymatic assays were performed at 30°C, following the formation of NADH at 340 nm.

2.2. Crystallization and X-ray diffraction data collection

Initial screening of crystallization conditions was carried out by the vapour-diffusion method using a Mosquito nanolitre dispensing system (TTP Labtech). Sitting drops were set up using 400 nl of a 1:1 mixture of each sample protein and crystallization solution (672 different commercially available conditions) equilibrated against 150 µl reservoir solution in multiwell plates (Greiner Bio-One). The crystallization plates were stored at 18°C in a Rock Imager 1000 (Formulatrix) automated imaging system to monitor crystal growth. Crystallization hits were improved by manually preparing hanging drops in 24-well plates at the same temperature, except for the D199N variant, where 4°C was used.

Optimized conditions for crystal growth were as follows. For the apo ΔCBS variant, the best crystals were obtained by mixing 1.5 µl protein solution at 9.2 mg ml^{-1} (in buffer *A*) with 1.5 µl reservoir solution consisting of either 4.3 *M* sodium chloride, 100 m*M* HEPES pH 7.5 or 10 m*M* sodium citrate, 33% PEG 8000. For the ΔCBS variant in complex with IMP, the best crystals were obtained by mixing 1.5 µl protein solution at 9.2 mg ml^{-1} (in buffer *A* with 10 m*M* IMP) with 1.5 µl reservoir solution consisting of 1.26 *M* ammonium sulfate, 100 m*M* HEPES pH 7.5. Finally, for the D199N variant in complex with IMP, the optimized crystals were obtained by mixing 1.5 µl protein solution at 11.7 mg ml^{-1} (in buffer *A* with 10 m*M* IMP) with 1.5 µl reservoir solution consisting of 10%(*w*/*v*) PEG 4000, 200 m*M* magnesium chloride, 100 m*M* MES pH 6.5.

Single crystals of the ΔCBS variant in its apo form and in complex with IMP were flash-cooled in liquid nitrogen using a mixture of 50% Paratone-N and 50% paraffin oil as a cryoprotectant. Crystals of the D199N variant in complex with IMP were flash-cooled in liquid nitrogen using a cryoprotectant mixture consisting of 75% crystallization solution and 25% glycerol.

All X-ray diffraction data were collected on the PROXIMA 1 beamline at the SOLEIL synchrotron, St Aubin, France. Diffraction images were integrated with *XDS* (Kabsch, 2010) and crystallographic calculations were carried out with programs from the *CCP*4 program suite (Winn *et al.*, 2011).

Table 1
Data-collection, phasing and refinement statistics for the structures of the IMPDHpa variants.

Values in parentheses are for the outer shell.

	ΔCBS	ΔCBS, IMP complex	D199N, IMP complex
PDB code	5ahl	5ahm	5ahn
Data collection			
Beamline	PROXIMA 1	PROXIMA 1	PROXIMA 1
No. of crystals	1	1	1
Space group	*I*422	*I*4	*I*4
Unit-cell parameters			
a (Å)	144.8	103.6	116.6
b (Å)	144.8	103.6	116.6
c (Å)	116.9	158.4	58.3
No. of molecules in asymmetric unit	1	2	1
Wavelength (Å)	0.98011	0.98011	0.98011
Resolution (Å)	1.95	1.74	1.65
R_{merge}† (%)	7.9 (47.8)	4.4 (43.7)	3.0 (45.0)
$\langle I/\sigma(I)\rangle$	21.9 (5.7)	13.1 (2.9)	20.1 (2.2)
Completeness (%)	100.0 (100.0)	99.5 (98.9)	98.6 (90.9)
Multiplicity	14.7 (14.5)	3.5 (3.4)	3.5 (2.6)
Wilson *B* factor (Å^2)	29.4	26.5	23.4
Refinement			
Resolution (Å)	45.5–1.95	43.3–1.75	38.8–1.65
No. of reflections	41840	152733	45339
R_{work}/R_{free}‡ (%)	16.6/20.5	15.7/18.5	15.5/17.7
No. of atoms			
Protein	2399	5308	2242
Ligand (IMP)	—	46	23
Ions	1	25	—
Water	423	592	361
B factors (Å^2)			
Protein	27.5	32.5	15.8
Ligand (IMP)	—	36.6	39.9
Ions	40.7	70.6	—
Water	43.9	43.5	35.7
R.m.s. deviations§			
Bond lengths (Å)	0.008	0.007	0.007
Bond angles (°)	1.079	1.051	1.087
Ramachandran plot (%)			
Most favourable	97.2	97.6	96.1
Allowed	2.8	2.1	2.9
Outliers	0.0	0.3	1.0

† $R_{merge} = \sum_{hkl}\sum_i |I_i(hkl) - \langle I(hkl)\rangle| / \sum_{hkl}\sum_i I_i(hkl) \times 100$. ‡ $R_{work} = \sum_{hkl} ||F_{obs}| - |F_{calc}|| / \sum_{hkl} |F_{obs}| \times 100$; R_{free} is calculated in the same way on a subset (5%) of reflections that were not used in refinement. § Deviation from ideal values.

2.3. Structure determination and refinement

Molecular replacement was performed using *MOLREP* (Vagin & Teplyakov, 2010). Rigid-body and restrained refinement was performed using *REFMAC*5 (Murshudov *et al.*, 2011), alternating with manual rebuilding in *Coot* (Emsley & Cowtan, 2004).

2.4. PDB accession codes

The refined models and structure factors have been deposited in the Research Collaboratory for Structural Biology Protein Data Bank (http://www.rcsb.org/) under the following accession numbers: 5ahl (ΔCBS apo form), 5ahm (ΔCBS variant complexed with IMP) and 5ahn (D199N variant complexed with IMP).

3. Results

The purification and the biochemical characterization of the two IMPDHpa variants studied here have been described previously (Labesse *et al.*, 2013). The ΔCBS variant lacks the CBS motifs from Ala92 to Lys202 of the full-length enzyme. This variant is fully active and its kinetic parameters are similar to those of wild-type IMPDHpa in the presence of its positive effector Mg-ATP (*i.e.* Michaelis kinetics for both substrates, high affinity for IMP, low affinity for NAD and high specific activity). The second variant harbours a point mutation at position 199 (D199N) within the second CBS motif. This aspartate residue, which is conserved in IMPDHs, has been shown to be involved in the recognition of the ribose moiety of ATP in IMPDHpa. The catalytic activity of the D199N variant is still sensitive to Mg-ATP, influencing both the maximal rate and the affinity for IMP, but the cooperativity effect for IMP is lost. The different properties of these two variants prompted us to engage in their structural characterization by means of X-ray crystallography.

3.1. Crystal structure of the ΔCBS variant in its apo form

High-resolution diffraction data were obtained from crystals grown in a high concentration of either a salt (4.3 *M* NaCl) or a large PEG (33% PEG 8000). The unit-cell parameters, merging statistics and systematic absences were consistent with space group *I*422. The computed Matthews coefficient (~2.8 Å^3 Da^{-1}) suggested that one monomer was present in the asymmetric unit. The crystals grown in the two distinct conditions appeared to be highly isomorphous, and structure refinement led to almost identical structures. Only the best structure (high-salt) was used for further analysis.

The structure of the ΔCBS variant was solved by molecular replacement using a previously solved structure of wild-type IMPDHpa (PDB entry 4dqw; Englert *et al.*, 2012) as a template and was refined to 1.95 Å resolution (Table 1). Beside the deleted CBS motifs, two large segments are not visible in the electron density. They correspond to the so-called flap loop (384–421 according to the numbering of IMPDHpa) and a C-terminal loop (467–487) (see Figs. 1*c* and 2). The rest of the catalytic domain is very well defined with good refinement parameters (R_{work} = 16.6%, R_{free} = 20.5%).

The fourfold symmetry gives rise to a tetrameric organization of the catalytic domains which is well conserved in all IMPDHs known to date. Globally, the tetramer of catalytic domains in the ΔCBS variant appears to be highly similar to those previously described for wild-type IMPDHpa in its various forms (*e.g.* PDB entries 4dqw, 4avf and 3zfh; Fig. 1*a*; Englert *et al.*, 2012; Moynie *et al.*, 2013; Rao *et al.*, 2013). Indeed, the r.m.s.d.s (computed over the stable core of the catalytic domains) are rather low (0.3–0.4 Å at the monomer level) and are close to the estimated positional error (~0.2 Å). Accordingly, deletion of the CBS motifs did not impact on the global structural organization of the catalytic domains (Fig. 1*a*).

Importantly, two tetramers face each other in the crystal and are related by the twofold symmetries perpendicular to

the fourfold axis. As recently shown, a survey of the crystal packing in the apo structures of other IMPDHs revealed a similar organization (Labesse *et al.*, 2013). Here, the deduced octameric organization appears to be maintained despite the absence of the CBS motifs. Nevertheless, the CBS motifs may provide a better stabilization of this octamer, as the ΔCBS variant shows a tetramer–octamer equilibrium in solution, while the full-length enzyme forms a stable octamer according to analytical ultracentrifugation measurements (Labesse *et al.*, 2013). Indeed, in this high-resolution structure of the ΔCBS variant apo form the tetramer–tetramer interface is apparently limited, being built up only by the so-called finger loop that forms a β-hairpin (residues 373–383) from each monomer (Fig. 3*a*). However, these data suggest that the catalytic domains also participate in the formation of an octameric state.

Within the isolated tetramer the four finger loops are well ordered, but they point into the solvent and show little or no interaction with the remainder of the macromolecule. On the contrary, within the octameric organization each finger loop interacts with an equivalent segment from another monomer protruding from a facing tetramer (Fig. 3*a* and Supplementary Figs. S1*a* and S1*c*). Notably, this apo form of the ΔCBS variant adopted an identical conformation in two totally distinct crystallization conditions (high-salt *versus* large PEG crystallization conditions). In addition, such contacting hairpins have been observed in the apo forms of various IMPDHs described to date (*e.g.* PDB entry 4avf), suggesting that the conformation is not owing to spurious crystal-packing constraints.

The potentially important role of this finger loop is in agreement with its high sequence conservation among most IMPDHs (Fig. 2). Several residues interacting with this β-hairpin also show good conservation. Accordingly, most of the residues lying at the tetramer–tetramer interface (Fig. 4*a*) are either rather well conserved (Arg56, Glu367, Leu375 and Ser383) or invariant (Arg379 and Tyr425). Notably, the finger loop lies near the catalytic site.

3.2. Crystal structure of the ΔCBS variant in its IMP-bound form

To better understand the role of the finger loop, we attempted to solve the structure of this variant in the presence of the substrate IMP alone or in the presence of the cofactor (NAD). Only the IMP-bound form led to nicely diffracting crystals in which the ligand was visible.

High-resolution diffraction data were collected from crystals grown in the presence of 1.26 *M* ammonium sulfate and 0.1 *M* HEPES buffer pH 7.5 at 18°C. The unit-cell parameters, merging statistics and systematic absences were consistent with space group *I*4. The computed Matthews coefficient (~1.9 Å^3 Da^{-1}) suggested that two monomers were present in the asymmetric unit.

The structure of the ΔCBS variant of IMPDH in its IMP-bound form was solved by molecular replacement using the apo form as a starting template and was refined to 1.74 Å resolution (Table 1). In the two independent monomers modelled in the asymmetric unit almost all of the catalytic domains are very well defined. The C-terminal loop (467–487) is now completely ordered as is most of the flap loop (residues 384–390 and 415–426), with only the tip of the flap (residues 391–414) still not visible (Fig. 3*b*). The refinement rapidly led to very good statistics (R_{work} = 15.7%, R_{free} = 18.5%)

Importantly, the nucleotide IMP is bound in the active site of the two crystallographically independent monomers. Its orientation matched that described previously in other IMPDHs

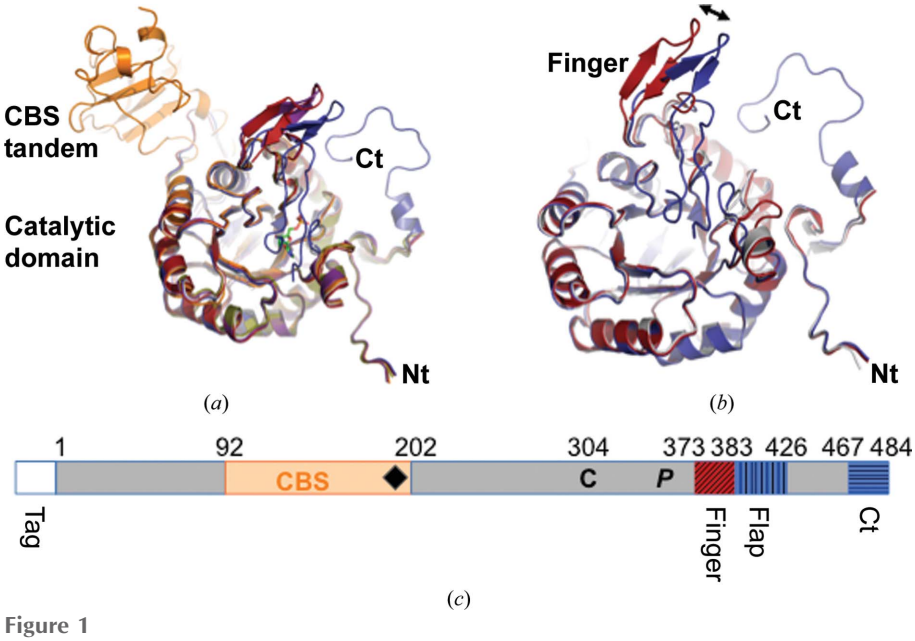

Figure 1
Structural comparison of the various monomeric structures of IMPDHpa, its point mutant D199N and its ΔCBS variant. (*a*) Superposed structures of the apo forms (wild-type enzyme, PDB entries 4avf and 3zfh in violet and green, respectively; ΔCBS variant, this study, in red), the Mg-ATP-bound form (PDB entry 4dqw, in orange) and the two IMP-bound forms (ΔCBS variant in dark blue and D199N variant in grey). The IMP molecule of the ΔCBS structure is shown as sticks (in CPK colours with C atoms in light green). (*b*) As in (*a*) but with only the three structures solved in this study in order to highlight the orientation shift (shown using a double arrow in black) of the flap loop between the apo form (red ribbons) and the IMP-bound form (blue ribbons). The structure of the IMP-bound D199N crystal structure is shown in grey ribbons to demonstrate the absence of significant change in the catalytic domain besides the two active-site loops (phosphate-binding and catalytic loops). The figure was generated by *PyMOL* (http://www.pymol.org). (*c*) IMPDHpa primary sequence as a schematic bar representation to position the CBS motifs (orange) and Asp199 (grey triangle), as well as important loops involved in the building of the active site: the catalytic loop (residues 299–306 around Cys304; indicated by C), phosphate-binding loop (residues 361–365; indicated by P), finger loop (residues 373–383; diagonal red stripes), flap loop (residues 384–421; vertical blue stripes) and C-terminal loop (residues 467–487; horizontal blue stripes). The N-terminal histidine tag is also shown (white box).

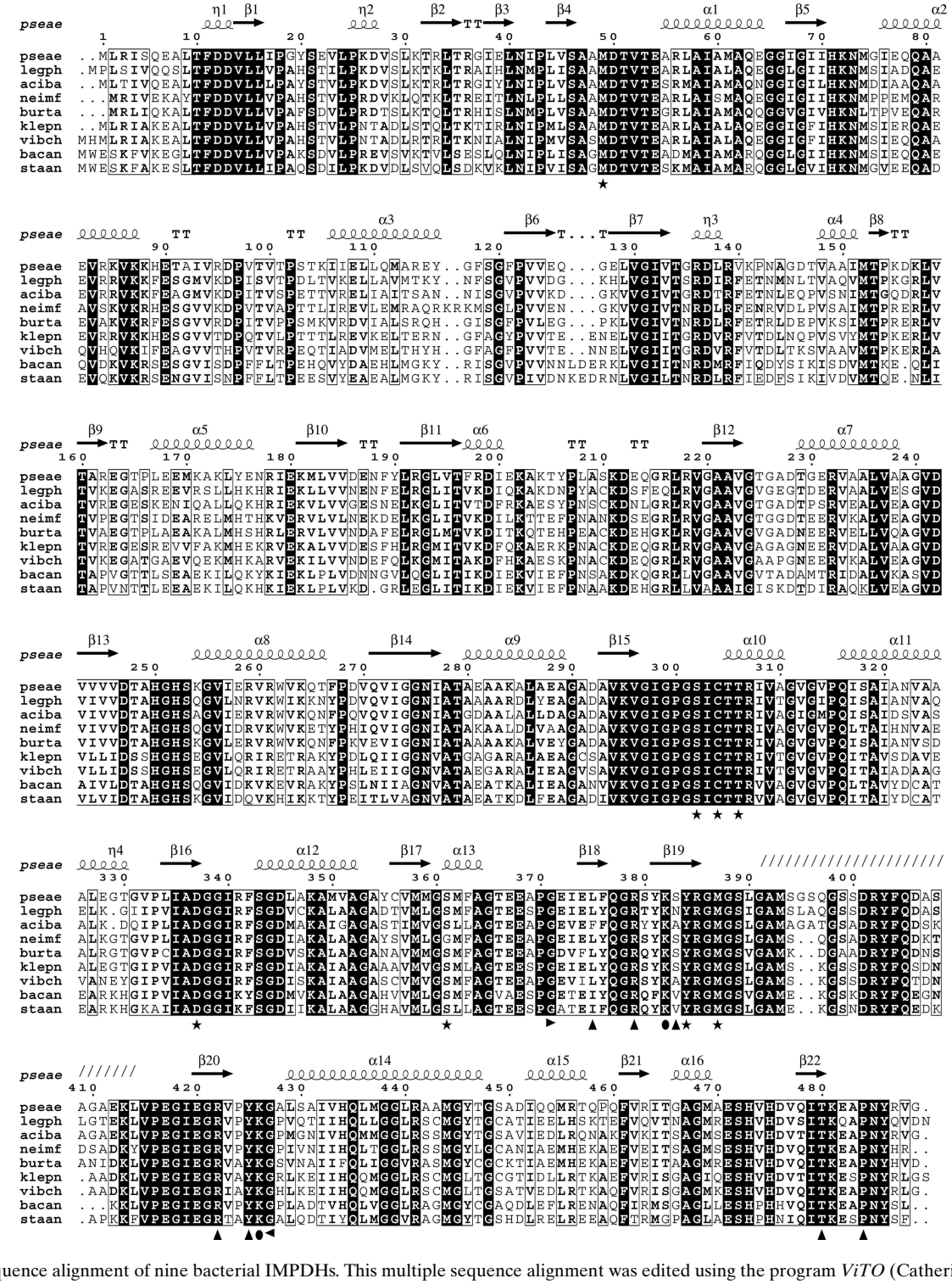

Figure 2
Complete sequence alignment of nine bacterial IMPDHs. This multiple sequence alignment was edited using the program *ViTO* (Catherinot & Labesse, 2004) and refined manually. Sequences are labelled according to their origin following the rules of SWISS-PROT naming [pseae, *P. aeruginosa*; legph, *Legionella pneumophila* subsp. *pneumophila* (strain Philadelphia-1); aciba, *Acinetobacter baumannii*; neimf, *Neisseria meningitidis*; burta, *Burkholderia thailandensis* (strain E264); klepn, *Klebsiella pneumoniae*; bacan, *Bacillus anthracis* (strain Sterne); vibch, *Vibrio cholerae*; staan, *Staphylococcus aureus* (strain N315)]. Secondary structures are highlighted above the sequence and include those observed in the CBS domains visible in the ATP-bound form of IMPDHpa (PDB entry 4dqw). The stretch of slashes (/) above the alignment highlights the segment 389–416, the structure of which has never been observed for IMPDHpa. The positions of important residues are indicated using black symbols depending on their role in IMP binding or the octameric interface: stars for the catalysis or recognition of the IMP molecule (*e.g.* residues 49, 302, 304 and 306), with upward triangles for residues at the tetramer–tetramer interface; left- and right-pointing triangles pinpoint two glycine residues (Gly371 and Gly426) delimiting the region that is not visible in the IMP-bound form of the D199N mutant; finally, filled circles highlight the two buried lysines (382 and 426) whose side chains interplay with the dynamic behaviour of the finger and flap loops (see text). The finger loop (residues 373–383) corresponds to a β-hairpin formed by two β-strands (β18 and β19), while the flap loop (residues 384–421) includes two extended segments (the end of strand β19 and strand β20) and a region not that is visible in the IMP-bound form (residues 391–414; dotted line above the alignment). The figure was generated by *ESPript* (Robert & Gouet, 2014).

(Prosise & Luecke, 2003). The rather short distance (2.6 Å) and the presence of residual electron density between the S^{γ} atom of Cys304 and the C2 atom of the substrate suggests that these two atoms are adequately oriented and ready to engage in a covalent connection (Fig. 4*c*). This is in agreement with the ΔCBS variant being catalytically competent. The nucleobase is recognized by residues from the ordered part of the flap loop, especially through the main-chain atoms of Met387, Gly388 and Glu417 (interacting with the N7, O6 and N1 atoms of the inosine moiety, respectively). In addition, the conserved Tyr384 from the flap loop is hydrogen-bonded to the phosphate moiety. The latter interacts mainly with the amide groups of residues Gly360 and Ser361 from the loop 360–364, the conformation of which is stabilized by the N atom of the Lys426 side chain. These interactions are highly conserved among various IMPDHs (data not shown).

Compared with the apo structure described above (§3.1), a rearrangement of the catalytic loop can be observed. It is

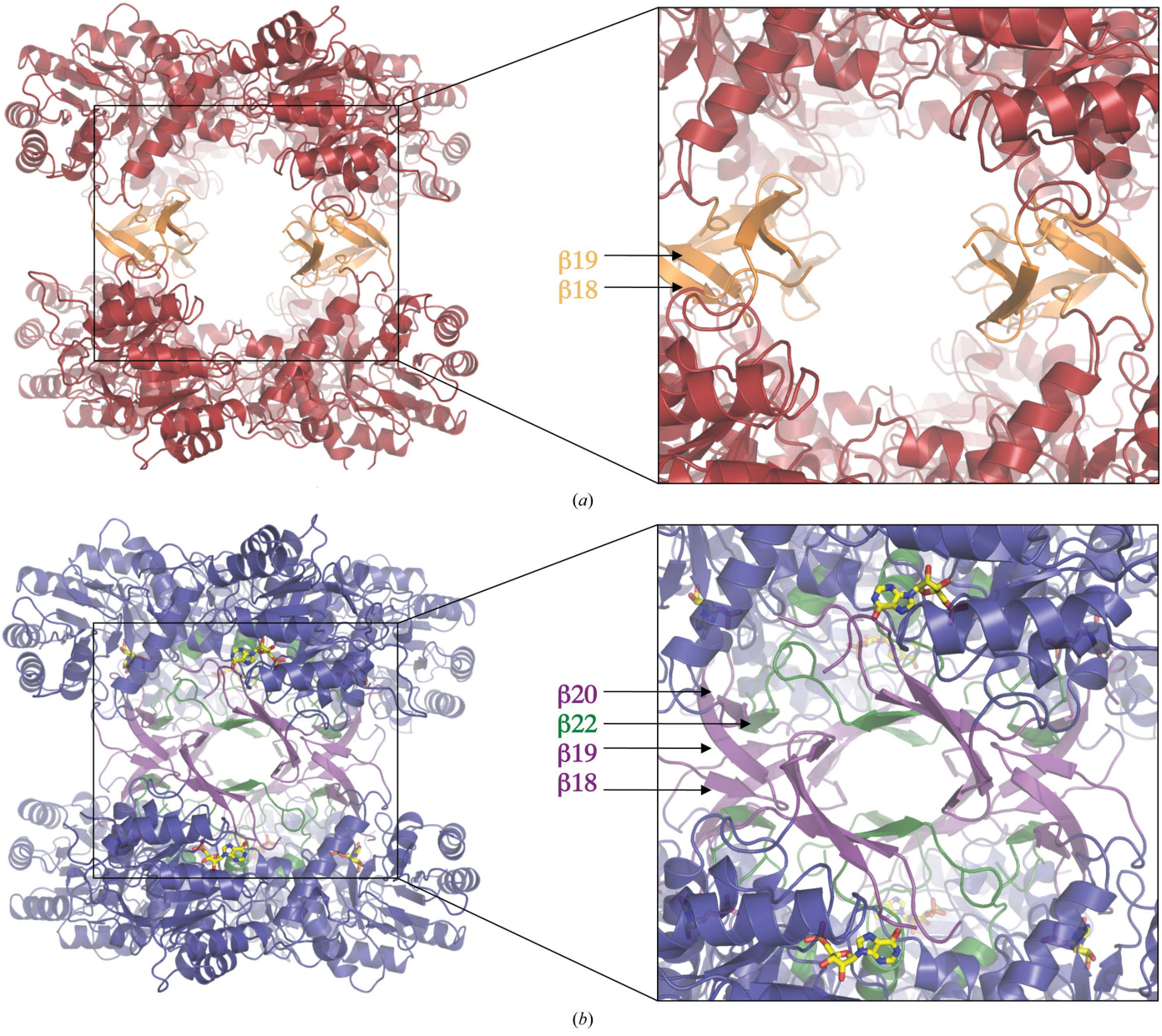

Figure 3
Structural comparison of the apo-form and the IMP-bound structures of the ΔCBS variant. (*a*) The octameric structure of the apo form is shown in red ribbons except for the interfaces, which are shown in yellow (*β*-strands *β*18 and *β*19 corresponding to the finger loop). (*b*) The octameric structure of the IMP-bound form is shown in ribbons coloured in blue (catalytic domains), green (C-terminus including *β*-strand *β*22) and purple (corresponding to the finger and flap loops including *β*-strands *β*18, *β*19 and *β*20). IMP molecules are shown in stick representation. Enlarged views of the interface regions are shown on the right, showing the structural elements involved in this interface (the *β*-strands of the hairpin, flap and C-terminal loops are labelled when visible) and highlighting their distinct arrangements in the presence or absence of IMP within the catalytic domain. The octameric structures were computed using *PISA* (Krissinel & Henrick (2007) and superposed using the program *SUPCOMB* (Kozin & Svergun, 2001). The figures were generated by *PyMOL* (http://www.pymol.org).

accompanied by stabilization of the C-terminal segment, which is otherwise not visible in the electron density (Fig. 3). Meanwhile, the finger loop shows a significant shift in its orientation, with a movement of up to 5 Å at its tip (Fig. 3). The β-hairpin (residues 378–380) is still in contact with the equivalent segment from a second monomer. In parallel, the ordered C-terminus from another monomer comes into close contact with the finger and the flap loops (Figs. 3 and 4*b*). This results in a new and small β-barrel with a network of hydrogen bonds between the backbone atoms of residues 480–482 (belonging to the C-terminal loop) and residues 374′–378′ (belonging to the β-hairpin) from the other monomer. Accordingly, stabilization of the octameric structure now involves, in addition to the finger and the flap loops, another important segment in the catalytic domain, its C-terminus.

Superposition of the catalytic domains of this IMP-bound form and the apo form shows a very low overall r.m.s.d. (∼0.4 Å). The main differences are in the organization of the loops around the active site (Fig. 1*b*). Compared with the apo structure described above (§3.1), the finger loop shows a significant shift in its orientation, with a movement of up to ∼6.5 Å at its tip (measured as the mean C^{α}–C^{α} distance of Gln377 and Gly378 in the apo and IMP-bound forms). This rearrangement is accompanied by a translation of the same amplitude for the small β-strand ranging from residues 373 to 375. As a result, the Leu375 side chain is no longer in contact with Ala431 and Ile432 from the last α-helix of the catalytic domain, but instead contacts the Pro484 side chain in the C-terminal tail. In addition, a hydrogen bond is formed by the backbone atoms of Leu375 and Glu382. This contact connects the β-hairpin of the finger loop from one monomer to a small β-strand (β22) present within the C-terminal tail of a second monomer. In turn, this β-strand forms a β-sheet with the two β-strands of the ordered flap loop (namely β19 and β20) from a third monomer. The latter monomer provides another finger loop that is also engaged in the formation of new β-sheet including β-strand β22 from a fourth monomer and the flap loop of the initial monomer. Thus, the structural rearrangement builds up a new eight-stranded β-barrel involving both the finger loop and the newly ordered segments (flap loop and C-terminus) in the IMP-bound form.

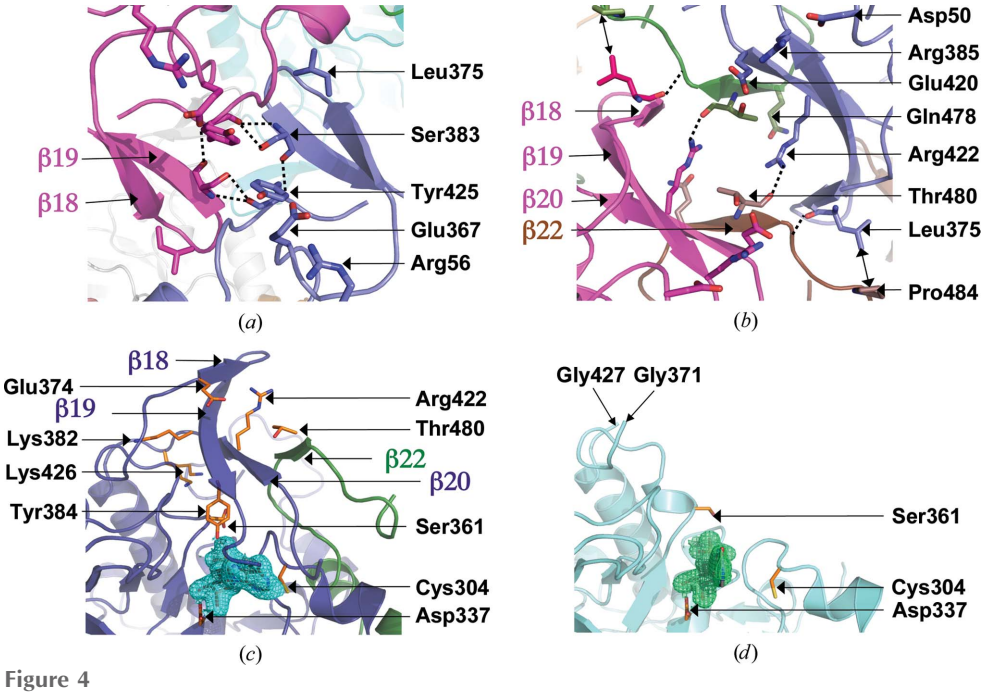

Figure 4
Interface and active-site rearrangements upon IMP binding in the ΔCBS variant. (*a*) and (*b*) show the interactions at the octameric interfaces of the apo form and the IMP-bound form of the ΔCBS variant, respectively. Important residues are shown in stick representation. The nonlabelled residues and β-strands are symmetry-related to the labelled ones. (*a*) In the foreground, the segments corresponding to the finger loops of two monomers facing each other in the octameric form are shown as pink and blue ribbons, respectively. Hydrogen bonds are shown as dotted lines and involve residues Ser383 (both backbone and side chain) and Tyr425 (backbone only). This interface is further stabilized by side-by-side interaction of the aromatic rings of the Tyr425 side chain, the conformation of which is maintained by a network involving two residues: Glu367 and Arg56. Additional hydrogen bonds at the finger–finger interface are formed by Ser383 and Tyr425 with the side chain of Arg379 pointing from each facing monomer in an alternating mode (not shown for clarity). In (*b*) four monomers (pink, blue, green and brown ribbons) are involved, and hydrogen bonds (dotted lines) or hydrophobic contacts (double-arrow lines) stabilizing this interface are shown. Residues shown as sticks are either directly involved in these interactions (Leu375, Arg422, Thr480 and Pro484) or in maintaining the observed conformation of the flap and finger loops (Asp50, Arg385 and Glu20 or Gln478). (*c*) Top view of the active site and neighbouring loops including the finger, the flap and the C-terminus in the IMP-bound form. The IMP molecule is shown in stick representation and the corresponding electron density is shown as a cyan surface and mesh. Residues stabilizing the local conformation (Glu374, Lys382, Arg422, Lys426 and Thr480) and/or interacting with the ligand (Cys304, Asp337, Ser361 and Tyr384) are shown as orange sticks. (*d*) As in (*c*) but for the D199N variant structure. Gly427 and Gly371 are indicated to position the region that is not visible in this structure. Three ligand-binding residues are shown (Asp337, Ser361 and the catalytic Cys304). The IMP molecule is shown in stick representation and the corresponding electron density is shown as a green surface and mesh. The orientation of the substrate nucleobase is not compatible with catalysis. The figures were generated by *PyMOL* (http://www.pymol.org).

Globally, four additional β-barrels appear at the interface between two facing tetramers in the crystal of IMP-bound IMPDHpa. Interestingly, a similar configuration (Supplementary Fig. S1*b*) is observed in the recently solved structure of a deletion mutant of IMPDH from *Vibrio cholerae* (PDB entry 4ix2; Center for Structural Genomics of Infectious Diseases, unpublished work). The rearrangement observed upon substrate binding led to a dramatically different interface and a ∼20° rotation of one tetramer relative to the other (by comparison with the apo form). Again, as in the case of the apo form, this quaternary structure is observed in the absence of

the CBS motifs. The involvement of both the C-terminus and the flap loop in the tetramer–tetramer interface suggests that the octameric organization may influence the function of this allosteric enzyme.

3.3. Crystal structure of the D199N point mutant in its IMP-bound form

The D199N variant was selected as it has lost its cooperativity for IMP and also corresponds to the natural human mutant regularly observed in the corresponding protein (D226N IMPDH1) found in individuals with severe retinopathy (adRP10).

High-resolution diffraction data were collected from a crystal grown in the presence of 10% PEG 4000, 0.2 *M* $MgCl_2$, 0.1 *M* MES buffer pH 7.0 at 4°C. The unit-cell parameters, merging statistics and systematic absences were consistent with space group *I*4. The calculated Matthews coefficient (∼1.8 Å^3 Da^{-1}) suggested that one monomer was present in the asymmetric unit. The structure of the D199N variant in complex with IMP was solved by molecular replacement using the apo form as a starting template and was refined to 1.65 Å resolution (Table 1). Owing to the fourfold symmetry one tetramer can be built, but no octamer can be deduced from this crystal structure, in marked contrast to the former structures. We have no clear explanation for this behaviour. In solution, this variant was found by size-exclusion chromatography and confirmed by analyical ultracentrifugation to be octameric in the presence of IMP as well as in its apo form (data not shown). In addition, a low-resolution structure (5.9 Å) of this variant in the presence of Mg-ATP adopts the same octameric conformation (R_{work} = ∼26.2%, R_{free} = ∼28.5%; data not shown) as the wild-type enzyme bound to Mn-ATP. Nevertheless, the overall structure of the catalytic domain appeared to be highly similar to that of other crystal structures of IMPDHpa (Fig. 1*b*), with r.m.s.d.s ranging from 0.32 to 0.46 Å (over a common core of ∼300 residues). None of the long loops lying in the vicinity of the active site (the finger, the flap and the C-terminus) are visible in the electron density, suggesting high flexibility of these three segments. A similar conclusion was drawn from the crystal structure of Mg-ATP-bound IMPDHpa (PDB entry 4dqw).

One IMP molecule appears to be bound in the active site of this variant. However, the nucleobase moiety of the bound nucleotide adopts an original orientation distinct from that previously described in other IMPDHs. Indeed, the heterocycle of the inosine is rotated by ∼80° compared with its orientation in the ΔCBS variant. As a result, the catalytic cysteine Cys304 does not appear to be ready to form a covalent bond to the inosine (S^{γ}–C2 distance of 7.0 Å) in the D199N variant (Fig. 4*d*). In addition, the catalytic loop is observed in two alternating conformations. One corresponds to the open conformation seen in the apo form, while the second resembles that in the closed conformation observed in the IMP-bound form of the ΔCBS variant. On the other hand, the ribose moiety and the phosphate group superpose perfectly in these two IMP-bound structures. Accordingly, the particular IMP-binding mode may prevent the ordering of the flap loop and may represent an intermediate step in the entrance of the nucleotide into the active site.

3.4. Comparison with the crystal structures of the activated form of IMPDHpa

The overall structures of the catalytic domains appear to be highly similar in the two variants (ΔCBS and D199N), and they also resemble that of the wild-type enzyme in its Mg-ATP-bound form (Labesse *et al.*, 2013). At the monomer level, the r.m.s.d. with the ATP-bound form was only slightly higher (∼0.5 Å) than that between the apo and IMP-bound forms. The main differences are in the ordering of several important loops as well as in the relative distance between the facing tetramers within the octamers. These changes can be seen by the height of the various octamers, which increases from ∼80 Å in the apo and IMP-bound forms of the ΔCBS variant to ∼100 Å in the Mg-ATP-bound form.

Further comparative analysis of the various structures of IMPDHpa solved to date highlighted the presence of several hinges at the stems of the finger and the flap loops. Interestingly, near the beginning and the end of the finger and flap loops, several glycine residues are present (Gly365, Gly371 and Gly427). Of note, the polypeptide chain cannot be modelled in several crystal structures (*e.g.* the ATP-bound wild type, the D199N mutant and an apo form) between residues Gly371 and Lys426, with the latter residue lying just prior to Gly427. A similar situation can be described for the C-terminus, as the electron density vanished in most crystal structures of IMPDHpa at Gly468 (apart from the IMP-bound ΔCBS variant). Importantly, these three glycines are highly conserved in IMPDH sequences (Fig. 2), as are the segments forming the finger, the flap and the C-terminal loops. This suggests that the structural and dynamic behaviour of these three elements is important for the function of these enzymes.

In the cases of the three glycines, Gly365, Gly371 and Gly427, structure comparisons showed backbone rearrangements depending on the bound states. Importantly, these local rearrangements propagate to the IMP-binding site through a complex network of interactions. This network mainly relies on two rather well conserved lysines (Lys382 and Lys426), the side chains of which appear to be buried and pointing towards various carbonyl backbones.

In the known apo forms, the terminal N^{ζ} atom of Lys382 is hydrogen-bonded to the surrounding carbonyl groups of Thr366, Glu367 and Ala369 (with distances ranging from 2.7 to 3.0 Å). It also weakly interacts with the carbonyl of Gly371 in these structures. In parallel, the carbonyl group of Ala364 is hydrogen-bonded to the N^{ζ} atom of Lys426 (with a distance of 2.6–2.8 Å) of the wild-type IMPDHpa (PDB entry 4avf) and the ΔCBS variant (this study), but not in the other structures. Meanwhile, the same N atom N^{ζ} of Lys426 is hydrogen-bonded to the carbonyl groups of Ser361 (distance of 2.9 Å) and Met362 (distance of 3.2 Å).

On the contrary, in the IMP-bound structure of the ΔCBS variant, the terminal N atom of Lys382 is farther from that of

Glu367 and is no longer in contact with the carbonyl of Gly371 owing to a movement of the latter residue (a 0.75 Å shift and a 80° rotation). This rearrangement is accompanied by a shift of the C^{α} atom of Gly365 by 2.35 Å and a 180° flip of the Ala364-Gly365 peptide bond. This prevents hydrogen bonding of Lys426 to Ala364 as observed in the apo form. In parallel, the Lys426 side chain is no longer interacting with Ser361 as the distance from the N^{ζ} atom to the carbonyl O atom increases to 4.3 Å upon IMP binding. Instead, the lysine is hydrogen-bonded to the carbonyl of Pro424.

In conclusion, substrate binding induces a coordinated rearrangement involving residues in the finger and flap loops (*e.g.* Lys382 and Lys426) and residues forming the phosphate-binding loop (mainly Ser361 and Met362). In parallel, the ordering of the C-terminus is concomitant with a stabilization of the catalytic loop (residues 302–306) in its active conformation. Accordingly, local structural changes occurring at the interface between several monomers (movement of the finger loop as well as ordering of the flap loop and the C-terminal tail) are connected to conformational changes in the active site.

4. Discussion

In this study, we have characterized the structures of two IMPDHpa variants that affect the allosteric behaviour. Our previous study suggested that the CBS motifs are highly important to stabilize the resting and activated octameric structures (Labesse *et al.*, 2013). They are also involved in the binding of the allosteric regulator Mg-ATP. The crystal structures of the ΔCBS variant indicate that IMPDH octamerization may not rely solely on the CBS motifs but may also involve the catalytic domains through interactions between several loop segments including the distorted C-terminus. In the deletion variant (this study) and in the apo form of the wild-type enzyme (PDB entry 4avf), the finger loop (residues 373–383 in IMPDHpa) seems to maintain this structural organization. It is in contact with the equivalent loop in the facing monomer (from a second tetramer). Furthermore, in the IMP-bound form this loop is also in contact with the C-terminal segment (481–482) and with the β-sheet of the flap loop wrapping onto the IMP-binding site. This suggests a network of concerted conformational changes connecting the tetrameric structure (mainly through the C-terminus) but also the octameric structure (mainly through the finger loops) with the catalytic site. The changes induced by Mg-ATP binding on the overall shape of the octamer may affect the functioning of the enzyme by perturbing the local flexibility and changing the balance between the unbound and bound forms, therefore affecting the catalytic turnover.

At the monomer level, the major changes correspond to the ordering or movement of the crucial loops for the catalytic activity: the finger, the flap and the C-terminal loops. Notably, none of these loops is ordered in the Mg-ATP-bound form of the wild-type enzyme. The same is true in the D199N structure and in one of the two apo-form structures of wild-type IMPDHpa solved to date (PDB entry 3zfh), in which no octamer could be deduced from the crystal packing. In contrast, the finger loop is ordered in the deletion variant in its apo form and in the second of the two apo forms of wild-type IMPDHpa (PDB entry 4avf). In the IMP-bound form, the concomitant ordering of two segments (the C-terminal and the flap loops), which are distant in sequence, is coordinated with a conformational change of the catalytic loop that brings the catalytic Cys304 into the vicinity of the C2 position of the nucleobase.

Our work has provided insights into the IMP-binding site of IMPDHpa. Our attempts to solve structures of the wild-type enzyme in its IMP-bound form have failed to date, as reported in the case of other bacterial IMPDHs. The ΔCBS variant of IMPDHpa constitutes an attractive truncated enzyme for high-resolution studies of ligand binding in the active site as observed for other IMPDHs (Makowska-Grzyska *et al.*, 2015). This opens the road to inhibitor screening targeting IMPDHpa.

Structural comparisons with another bacterial IMPDH, the CBS motifs of which were also deleted (see Supplementary Fig. S1), suggested that the rearrangements observed in IMPDHpa are not merely owing to a particular crystal packing. This extends our previous structural survey highlighting conserved conformational changes in other IMPDHs at the octameric level (Labesse *et al.*, 2013). These results suggest that the relevant macromolecular organization of IMPDHs is as a dimer of tetramers and not isolated tetramers. This matches recent results from *in vivo* cross-linking experiments analysed by mass spectrometry showing the bridging of Lys157 from one monomer to that of another monomer (Navare *et al.*, 2015). According to the length of the linker (35 Å), this bridge cannot form in the tetrameric state (Lys157–Lys157′ distance of ∼100 Å) and therefore the octameric form is expected to exist *in vivo*.

From this structural study, one may deduce that the role of the CBS motifs is to prevent interactions between the finger loops as well as the ordering of the flap loops and C-termini in the activated state. This could facilitate the release or entrance of the substrate or the reaction product upon activation, *i.e.* by Mg-ATP binding to the CBS motifs. On the contrary, in the resting state the ligand-bound state may be more stable owing to loop ordering. This may ensure proper recognition and accurate orientation of the ligands (IMP, water and NAD) at each step of the complex catalytic cycle. However, these functional requirements may decrease the enzymatic turnover at low substrate concentrations. Accordingly, the inhibitory role of the CBS module in the absence of Mg-ATP may rely on too strong a stabilization of the various conformations that the active site adopts during a catalytic cycle.

Acknowledgements

We would like to thank Martin Cohen-Gonsaud for helpful discussions, Thomas J. Dougherty and Stephen Lory for critical reading of the manuscript and Patrick Weber for performing robot-driven crystallizations trials. We acknowledge SOLEIL for provision of synchrotron-radiation facilities, and we thank the staff of beamline PROXIMA 1 for assis-

tance. The authors acknowledge financial support from the CNRS, INSERM and the Institut Pasteur. TA was a recipient of a PhD fellowship from the Conseil Régional d'Ile-de-France and the 'D.I.M. maladies infectieuses, parasitaires et nosocomiales émergentes' 2011. The authors also acknowledge support from the French Infrastructure for Integrated Structural Biology (FRISBI) ANR-10-INSB-05-01.

References

Aherne, A., Kennan, A., Kenna, P. F., McNally, N., Lloyd, D. G., Alberts, I. L., Kiang, A.-S., Humphries, M. M., Ayuso, C., Engel, P. C., Gu, J. J., Mitchell, B. S., Farrar, G. J. & Humphries, P. (2004). *Hum. Mol. Genet.* **13**, 641–650.

Bateman, A. (1997). *Trends Biochem. Sci.* **22**, 12–13.

Bowne, S. J., Sullivan, L. S., Blanton, S. H., Cepko, C. L., Blackshaw, S., Birch, D. G., Hughbanks-Wheaton, D., Heckenlively, J. R. & Daiger, S. P. (2002). *Hum. Mol. Genet.* **11**, 559–568.

Bowne, S. J., Sullivan, L. S., Mortimer, S. E., Hedstrom, L., Zhu, J., Spellicy, C. J., Gire, A. I., Hughbanks-Wheaton, D., Birch, D. G., Lewis, R. A., Heckenlively, J. R. & Daiger, S. P. (2006). *Invest. Ophthalmol. Vis. Sci.* **47**, 34–42.

Catherinot, V. & Labesse, G. (2004). *Bioinformatics*, **20**, 3694–3696.

Chen, L. & Pankiewicz, K. W. (2007). *Curr. Opin. Drug Discov. Devel.* **10**, 403–412.

Emsley, P. & Cowtan, K. (2004). *Acta Cryst.* D**60**, 2126–2132.

Englert, M., Xia, S., Okada, C., Nakamura, A., Tanavde, V., Yao, M., Eom, S. H., Konigsberg, W. H., Söll, D. & Wang, J. (2012). *Proc. Natl Acad. Sci. USA*, **109**, 15235–15240.

Ereño-Orbea, J., Oyenarte, I. & Martínez-Cruz, L. A. (2013). *Arch. Biochem. Biophys.* **540**, 70–81.

Goldstein, B. M., Risal, D. & Strickler, M. (2003). *Inosine Monophosphate Dehydrogenase: A Major Therapeutic Target*, edited by K. W. Pankiewicz & B. M. Goldstein, pp. 140–168. Washington: American Chemical Society.

Hedstrom, L. (2009). *Chem. Rev.* **109**, 2903–2928.

Hedstrom, L., Liechti, G., Goldberg, J. B. & Gollapalli, R. (2011). *Curr. Med. Chem.* **18**, 1909–1918.

Kabsch, W. (2010). *Acta Cryst.* D**66**, 125–132.

Kennan, A., Aherne, A., Palfi, A., Humphries, M., McKee, A., Stitt, A., Simpson, D. A., Demtroder, K., Orntoft, T., Ayuso, C., Kenna, P. F., Farrar, G. J. & Humphries, P. (2002). *Hum. Mol. Genet.* **11**, 547–557.

Kozhevnikova, E. N., van der Knaap, J. A., Pindyurin, A. V., Ozgur, Z., van Ijcken, W. F., Moshkin, Y. M. & Verrijzer, C. P. (2012). *Mol. Cell*, **47**, 133–139.

Kozin, M. B. & Svergun, D. I. (2001). *J. Appl. Cryst.* **34**, 33–41.

Krissinel, E. & Henrick, K. (2007). *J. Mol. Biol.* **372**, 774–797.

Labesse, G., Alexandre, T., Vaupré, L., Salard-Arnaud, I., Him, J. L. K., Raynal, B., Bron, P. & Munier-Lehmann, H. (2013). *Structure*, **21**, 975–985.

Makowska-Grzyska, M., Kim, Y., Maltseva, N., Osipiuk, J., Gu, M., Zhang, M., Mandapati, K., Gollapalli, D. R., Gorla, S. K., Hedstrom, L. & Joachimiak, A. (2015). *J. Biol. Chem.* **290**, 5893–5911.

Mortimer, S. E. & Hedstrom, L. (2005). *Biochem. J.* **390**, 41–47.

Moynie, L., Schnell, R., McMahon, S. A., Sandalova, T., Boulkerou, W. A., Schmidberger, J. W., Alphey, M., Cukier, C., Duthie, F., Kopec, J., Liu, H., Jacewicz, A., Hunter, W. N., Naismith, J. H. & Schneider, G. (2013). *Acta Cryst.* F**69**, 25–34.

Murshudov, G. N., Skubák, P., Lebedev, A. A., Pannu, N. S., Steiner, R. A., Nicholls, R. A., Winn, M. D., Long, F. & Vagin, A. A. (2011). *Acta Cryst.* D**67**, 355–367.

Nair, V. & Shu, Q. (2007). *Antivir. Chem. Chemother.* **18**, 245–258.

Navare, A. T., Chavez, J. D., Zheng, C., Weisbrod, C. R., Eng, J. K., Siehnel, R., Singh, P. K., Manoil, C. & Bruce, J. E. (2015). *Structure*, **23**, 762–773.

Nimmesgern, E., Black, J., Futer, O., Fulghum, J. R., Chambers, S. P., Brummel, C. L., Raybuck, S. A. & Sintchak, M. D. (1999). *Protein Expr. Purif.* **17**, 282–289.

Pankiewicz, K. W. & Goldstein, B. M. (2003). *ACS Symp. Ser.* **839**, 1–17. doi:10.1021/bk-2003-0839.ch001.

Pimkin, M. & Markham, G. D. (2008). *Mol. Microbiol.* **68**, 342–359.

Pimkin, M., Pimkina, J. & Markham, G. D. (2009). *J. Biol. Chem.* **284**, 7960–7969.

Prosise, G. L. & Luecke, H. (2003). *J. Mol. Biol.* **326**, 517–527.

Rao, V. A., Shepherd, S. M., Owen, R. & Hunter, W. N. (2013). *Acta Cryst.* F**69**, 243–247.

Ratcliffe, A. J. (2006). *Curr. Opin. Drug Discov. Devel.* **9**, 595–605.

Robert, X. & Gouet, P. (2014). *Nucleic Acids Res.* **42**, W320–W324.

Rose, P. W., Beran, B., Bi, C., Bluhm, W. F., Dimitropoulos, D., Goodsell, D. S., Prlic, A., Quesada, M., Quinn, G. B., Westbrook, J. D., Young, J., Yukich, B., Zardecki, C., Berman, H. M. & Bourne, P. E. (2011). *Nucleic Acids Res.* **39**, D392–D401.

Scott, J. W., Hawley, S. A., Green, K. A., Anis, M., Stewart, G., Scullion, G. A., Norman, D. G. & Hardie, D. G. (2004). *J. Clin. Invest.* **113**, 274–284.

Shu, Q. & Nair, V. (2008). *Med. Res. Rev.* **28**, 219–232.

Thomas, E. C., Gunter, J. H., Webster, J. A., Schieber, N. L., Oorschot, V., Parton, R. G. & Whitehead, J. P. (2012). *PLoS One*, **7**, e51096.

Vagin, A. & Teplyakov, A. (2010). *Acta Cryst.* D**66**, 22–25.

Winn, M. D. *et al.* (2011). *Acta Cryst.* D**67**, 235–242.